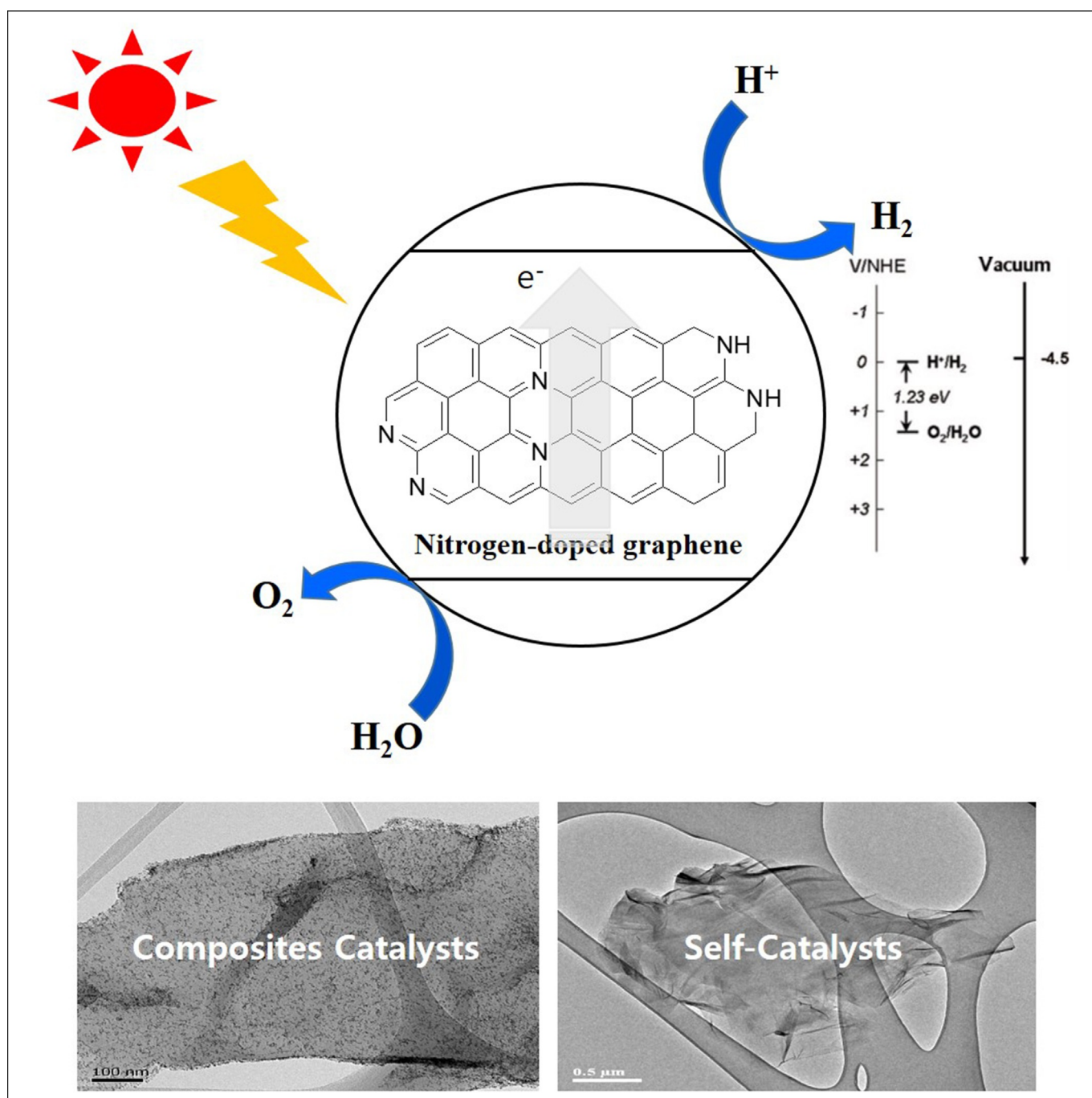


Photocatalytic Hydrogen Generation

SPECIAL ISSUE Nitrogen-Doped Graphene for Photocatalytic Hydrogen Generation

Dong Wook Chang^{*[a]} and Jong-Beom Baek^{*[b]}



Abstract: Photocatalytic hydrogen (H₂) generation in a water splitting process has recently attracted tremendous interest because it allows the direct conversion of clean and unlimited solar energy into the ideal energy resource of H₂. For efficient photocatalytic H₂ generation, the role of the photocatalyst is critical. With increasing demand for more efficient, sustainable, and cost-effective photocatalysts, various types of semiconductor photocatalysts have been intensively developed. In particular, on the basis of its superior catalytic and tunable electronic properties, nitrogen-doped graphene is a potential candidate for a high-performance photocatalyst. Nitrogen-doped graphene also offers additional advan-

tages originating from its unique two-dimensional sp²-hybridized carbon network including a large specific surface area and exceptional charge transport properties. It has been reported that nitrogen-doped graphene can play diverse but positive functions including photo-induced charge acceptor/mediator, light absorber from UV to visible light, n-type semiconductor, and giant molecular photocatalyst. Herein, we summarize the recent progress and general aspects of nitrogen-doped graphene as a photocatalyst for photocatalytic H₂ generation. In addition, challenges and future perspectives in this field are also discussed.

1. Introduction

To solve emerging energy and environmental issues and problems, the development of clean and renewable energy resources has attracted a great deal of interest in both academia and industry. Above all, solar light is receiving attention owing to its remarkable potential as an everlasting and cost-effective renewable energy resource. The conversion of solar energy into alternative fuels generally takes place through two representative pathways, photovoltaic^[1] and photocatalytic processes.^[2] The former is related to direct conversion of solar light into electric energy, while the latter refers to the production of hydrogen (H₂) or hydrocarbon fuel during the photocatalytic reaction of water (H₂O) or carbon dioxide (CO₂), respectively. Recently, H₂ is considered an ideal energy resource, because it can not only provide a high energy yield but also freedom from undesirable CO₂ generation during combustion.^[3] However, the current production of H₂ is strongly dependent on the conventional steam reforming process of fossil fuels, which is inadequate to meet emerging demands for unlimited and clean energy resources.^[4] Therefore, the evolution of H₂ by using a photocatalytic water splitting process under sunlight is of great importance. Although various semiconductor photocatalysts have been developed to date, the exploration of more efficient, sustainable, and cost-effective photocatalysts is still highly demanded.^[5]


Graphene, a one-atom thick single layer of graphite with a two-dimensional sp²-hybridized carbon structure, has attract-

ed enormous attention due to its unique properties such as high mechanical strength, superior thermal conductivity, outstanding transparency, huge specific surface area, and excellent charge transport.^[6] As such, graphene can be considered an ideal material for various fields including energy conversion and storage. However, further modulation of its intrinsic properties is strongly required to meet the rapidly increasing demand for practical applications in various fields.^[7] In this regard, chemical doping of heteroatoms such as boron (B) and nitrogen (N) is one of the most feasible approaches to tailor the diverse properties of graphene. For example, the broken lattice symmetry of graphene by additional heteroatoms can open a band gap and allow it to show semiconducting properties. In addition, fewer valence electrons of boron (B) and more valence electrons of nitrogen (N) can cause p-type and n-type conductive behaviors in graphene, respectively.^[8] Interestingly, the formation of active regions by asymmetric spin and charge distributions during heteroatom-doping in the graphene network can significantly improve the catalytic activity of doped graphene toward electrocatalytic or photocatalytic reactions.^[9] Much attention has been devoted to nitrogen-doped graphene, due to its several advantages including more facile synthetic protocols compared to its counterparts and superior performance in promising applications including supercapacitors, field-effect transistors, fuel cells and photocatalysts.^[9]

With unique advantages including large surface area, excellent electrical conductivity, a high population of active binding or catalytic sites, and tunable electronic properties, nitrogen-doped graphene is considered an ideal photocatalyst for photocatalytic H₂ generation.^[10] First, nitrogen-doped graphene can be used as a supporting matrix of semiconductor-based photocatalysts to enhance photocatalytic activity.^[11] In this configuration, the photo-induced charge separation, migration, and collection can be greatly improved by strengthened interfacial interactions as well as the formation of p-n heterojunctions between semiconductors and nitrogen-doped graphene. Second, nitrogen-doped graphene also shows great potential in metal-free photocatalysts based on their unique semiconducting and catalytic properties.^[12] Herein, we focus on recent advances of photocatalysts based on nitrogen-doped graphene for photocatalytic H₂ generation. Furthermore, remain-

[a] Prof. D. W. Chang
Department of Industrial Chemistry
Pukyung National University
365 Sinseon-ro, Busan 608-739 (South Korea)
E-mail: dwchang@pknu.ac.kr

[b] Prof. J.-B. Baek
School of Energy and Chemical Engineering/Low-Dimensional Carbon Materials Center
Ulsan National University of Science and Technology (UNIST)
100 Banyeon, Ulsan 689-798 (South Korea)
E-mail: jbbak@unist.ac.kr

 This manuscript is part of a special issue on energy conversion and storage. Click here to see the Table of Contents of the special issue.

ing challenges with nitrogen-doped graphene-based photocatalysts for photocatalytic H₂ generation are discussed.

2. Photocatalytic Hydrogen Generation

Since being discovered by Honda and Fujishima in 1972,^[2a] photocatalytic H₂ generation through a water splitting process has attracted tremendous attention. In this process, the most clean and abundant resources on the earth, sunlight and water, can be directly converted into the promising alternative fuel of H₂. The first electrochemical cell developed for a photocatalytic water splitting process employed a TiO₂ semiconductor and platinum for the photoanode and cathode, respectively.^[2a] The evolution of H₂ in an electrochemical cell involves the following four consecutive steps: the generation of electron (e⁻)-hole (h⁺) pairs on the photoanode by irradiation of sunlight, anodic oxidation of water to produce O₂ and H⁺ by photo-generated holes, the migration of photo-generated electrons to the cathode, and cathodic reduction of H⁺ to yield H₂ by accumulated electrons. Basically, the mixture of hydrogen (H₂)/oxygen (O₂) with a molar ratio of 2:1 can be produced during the water splitting process with a combination of anodic oxidation (H₂O + 2h⁺ → 2H⁺ + 1/2O₂) and cathodic reduction (2H⁺ + 2e⁻ → H₂).

For successful H₂ generation by the water splitting process, the role of photocatalyst is critical. As shown in Figure 1, the conduction band (CB) of the semiconductor should be located at a more negative potential than the reduction potential of H⁺/H₂ (0.0 V vs. NHE), while the location of the valence band (VB) must be more positive than the oxidation potential of OH⁻/O₂ (1.23 V vs. NHE).^[5a] In addition to the band position, the band gap of the semiconductor can also play an important role for efficient utilization of solar energy. A narrower band gap is usually preferred for the high conversion of solar energy, which is quite similar to the requirement of semiconductors in photovoltaic applications.^[13] As a result, the proper band gap of the semiconductor photocatalyst for the photocatalytic water splitting process is estimated to be in a range of 1.6 to 2.2 eV.^[14]

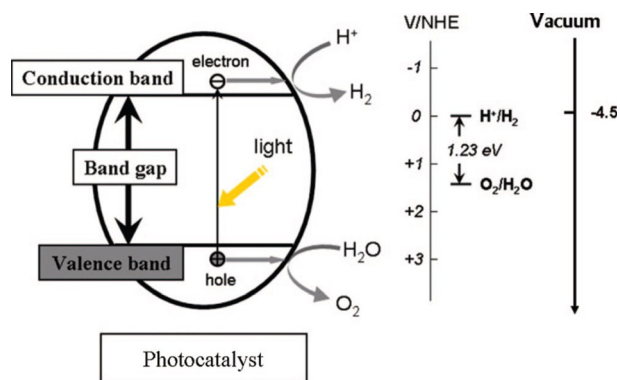


Figure 1. Illustration of the principle of the photocatalytic water splitting process on a semiconductor photocatalyst. Adapted from Ref. [5a] with permission, American Chemical Society.

Apart from band structures, other properties of photocatalysts also can be taken into account to enhance the photocatalytic performance in a water splitting process. Higher electrical conductivity is strongly recommended for the photocatalyst to diminish undesirable recombination of photo-induced electrons and holes through fast photo-induced charge separation and migration. Good resistance against photo-corrosion is also important for the long-term durable operation of the photocatalyst. Thus far, numerous semiconductor photocatalysts such as metal oxides (e.g., TiO₂, ZnO, Fe₂O₃), metal sulfides (e.g., CdS, ZnS) and carbon nitride (C₃N₄) have been applied to the photocatalytic water splitting process.^[3,5a] However, the overall performance is still far from ideal for practical applications and further research on more efficient, sustainable, and cost-effective photocatalysts is still highly required.

In this regard, several approaches have been developed for improving the performance of semiconductor photocatalysts, including loading of active metals,^[15] doping of suitable heteroatoms,^[16] and appropriate morphological controls.^[17] In addition, the concept of a heterojunction composed of multi-component catalysts, which was also successfully verified in photoelectrochemical and photovoltaic devices,^[18] has been intensively employed in the photocatalytic water splitting process.^[14] The efficiency and stability of the photocatalyst in the water splitting process can be significantly enhanced through effective separation and migration of photo-induced electrons and holes at the heterojunction structure. Some promising configurations of heterojunctions including Schottky, a p-n het-

Dong Wook Chang is an Assistant Professor in the Department of Industrial Chemistry at Pukyong National University, South Korea, since September 2014. Prior to joining his current position, he worked as a Research Assistant Professor at Ulsan National University of Science and Technology (UNIST, 2010-2012) and as an Assistant Professor in the Department of Chemical Systematic Engineering at the Catholic University of Daegu, South Korea (2012-2014). Currently, his research interests include the synthesis and functionalization of organic conjugated materials and graphene for energy conversion and storage.



Jong-Beom Baek is a Professor of School of Energy & Chemical Engineering at Ulsan National Institute of Science and Technology (UNIST), South Korea and a Director of Center for Dimension-Controllable Organic Framework. After receiving his PhD in Polymer Science from the University of Akron (USA) in 1998, he joined the Wright-Patterson Air Force Research Laboratory (AFRL). After four years at the AFRL, he returned to Korea as an Assistant Professor of Chemical Engineering at Chungbuk National University (Korea) in 2003, before moving to UNIST in 2008. His current research interests are the syntheses of high-performance covalent organic frameworks and the chemical modifications of carbon-based materials for multifunctional applications.



erojunction, a p-n heterojunction with an Ohmic layer, and a bulk heterojunction have been proposed in Figure 2.^[14]

Recently, carbon-based nanomaterials such as zero-dimensional fullerene, one-dimensional carbon nanotubes (CNTs) and two-dimensional graphene have attracted tremendous interest in the field of photocatalysts,^[10c,19] due to their unique advantages of excellent electrical conductivity, large surface area, and high stability. They can play diverse but positive functions including a photo-induced charge acceptor/mediator, a light absorber from UV to visible light, an n-type semiconductor, and a giant molecular photocatalyst.^[10b]

3. Synthesis of Nitrogen-Doped Graphene

With increasing demand for nitrogen-doped graphene for various applications,^[9] the synthesis of nitrogen-doped graphene with tailored properties becomes of great importance. Hitherto, a number of approaches have been intensively developed for the synthesis of high-quality nitrogen-doped graphene, including chemical vapor deposition (CVD),^[20] hydrothermal processes^[21] and heat/plasma treatment of graphene oxide (GO).^[22] The nitrogen atoms in the graphitic network usually exhibit three bonding configurations of quaternary N (graphitic N), pyrrolic N, and pyridinic N (Figure 3).^[23] As found for the oxygen reduction reaction (ORR),^[22a,24] the types and populations of each component in nitrogen-doped graphene can play crucial roles in determining the properties and performance of electrocatalysts. Therefore, selective formation of nitrogen configurations in graphitic networks have attracted remarkable attention to optimize structure–property relationships of nitrogen-doped graphene.^[25]

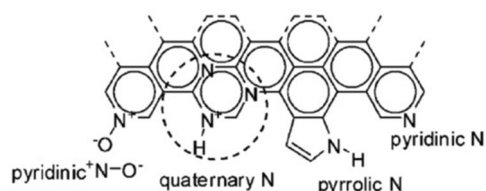


Figure 3. Bonding configurations of nitrogen atoms in nitrogen-doped graphene. Adapted from Ref. [23] with permission, Springer.

In addition, large preservation of typical sp^2 -hybridized graphitic networks in nitrogen-doped graphene is also critical, because the presence of damaged structures and/or defects can significantly deteriorate the unique properties of graphene such as its electrical conductivity. In this regard, edge-selectively functionalization of graphene can be considered a promising approach to produce high-quality nitrogen-doped graphene.^[26] In edge-selectively functionalized graphene (EFG), high populations of nitrogen atoms are mainly located on the reactive edges, while the crystalline graphitic structures in the basal plane are largely preserved. Recently, several methods have been developed to produce nitrogen-doped EFG including a direct Friedel–Crafts acylation in a mild PPA/ P_2O_5 medium^[27] and a mechanochemical ball-milling process.^[28] The Friedel–Crafts acylation reaction between pristine graphite and 4-aminobenzoic acid can produce 4-aminobenzoyl edge-functionalized graphene (EFG) and the subsequent heat treatment of EFG can lead to its transformation to N-graphene (Figure 4A). The mild acidic nature of the PPA/ P_2O_5 medium minimizes the structural damage of EFG during the reaction. As a result, the

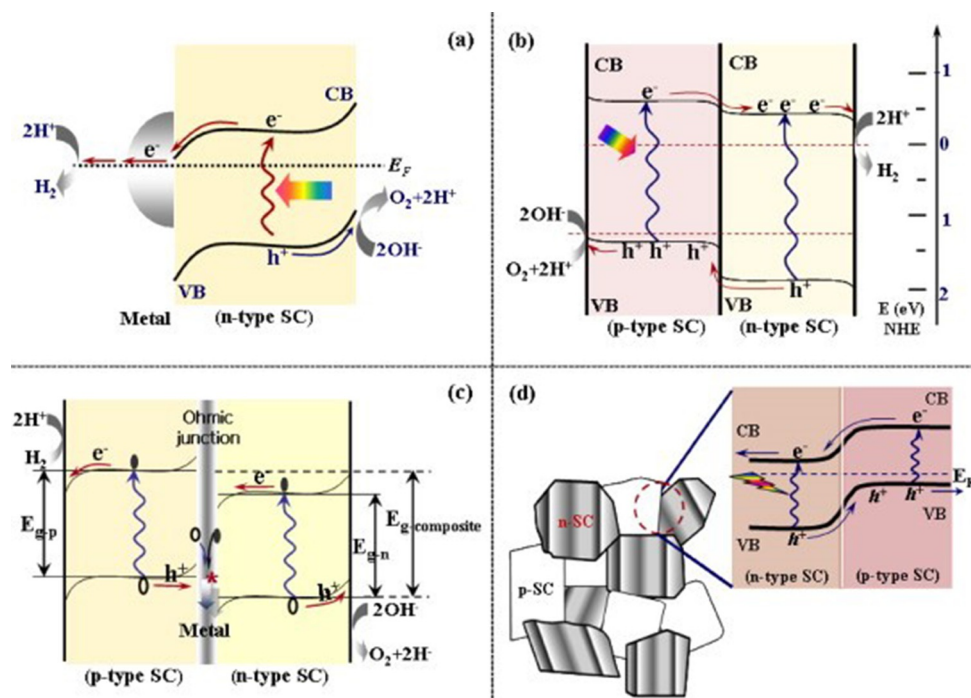


Figure 2. Schematic summary of (a) Shottky, (b) p-n heterojunction, (c) p-n heterojunction with Ohmic layer, and (d) bulk heterojunction in photocatalysts. Adapted from Ref. [14] with permission, Elsevier.

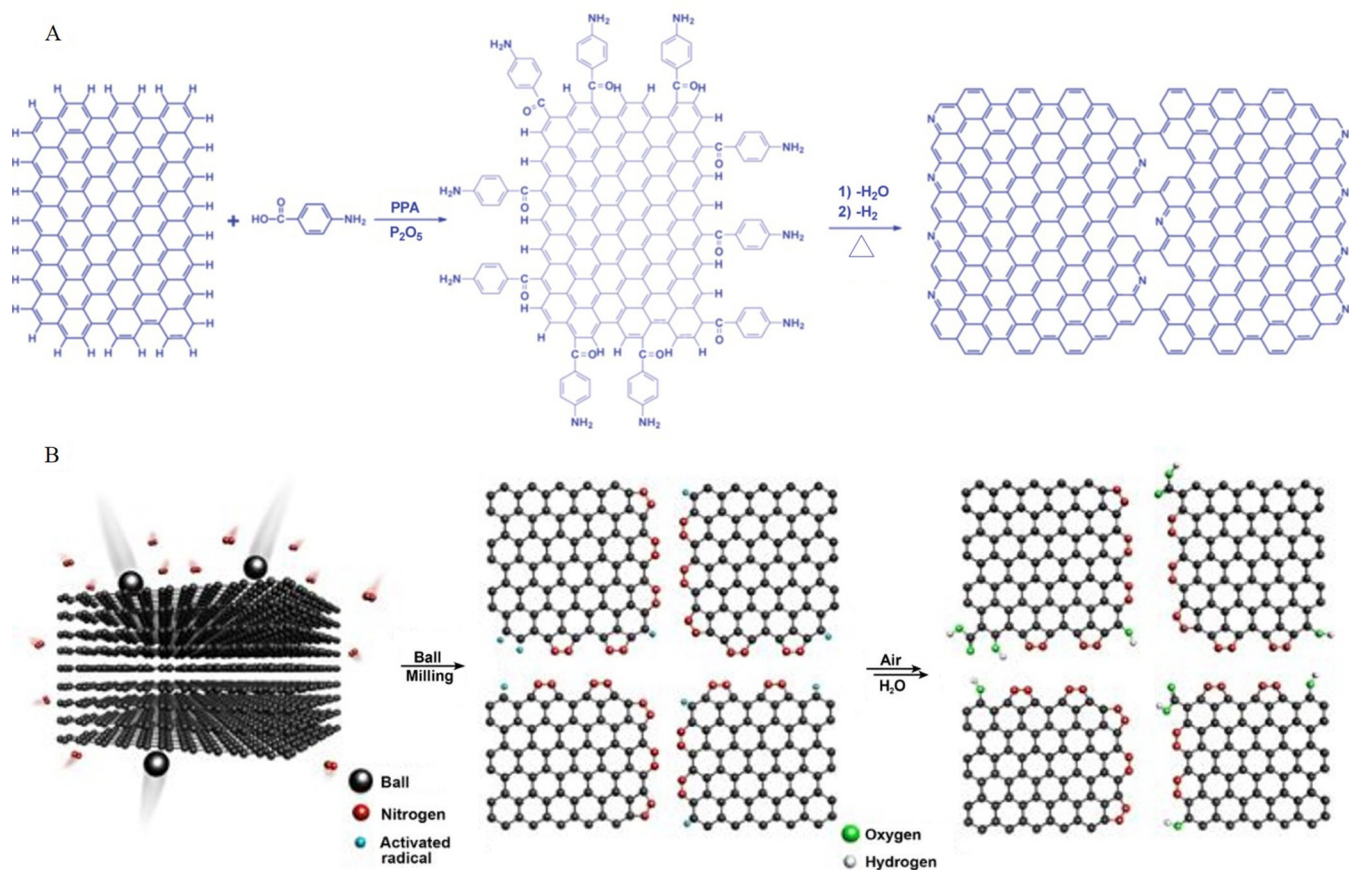


Figure 4. A) Schematic representations of EFG obtained by a Friedel–Crafts acylation reaction and subsequent heat treatment. B) Schematic illustrations of physical cracking of a graphite flake in a ball-mill crusher containing steel balls in the presence of nitrogen to produce NGnPs. Adapted from Ref. [27and28] with permission, American Chemical Society and National Academy of Sciences.

large-area film of N-graphene displays low sheet resistance (as low as $60 \Omega \text{sq}^{-1}$) and outstanding electrocatalytic activity toward the oxygen reduction reaction (ORR).^[27] Jeon et al. also reported direct nitrogen fixation at the edge of graphene to produce the edge-nitrogenated graphene (NGnPs) via ball milling of pristine graphite under a nitrogen atmosphere.^[28] The mechanochemical cleavage of graphitic C–C bonds by ball milling can generate active carbon species to react with nitrogen (Figure 4B). Both aromatic 5-membered pyrazole and 6-membered pyridazine rings at the edges of NGnPs are usually produced by the breakage of zigzag and armchair edge-cracking in graphite, respectively. Distortion of the basal plane has not been observed in NGnPs. Finally, the superb catalytic performance of NGnPs has been proven by both dye-sensitized solar cells (DSSCs) and fuel cells. These promising results obtained by EFG produced by either a direct Friedel–Crafts acylation or a mechanochemical ball-milling process reflect the strong potential of EFG for the development of high-quality nitrogen-doped graphene for various applications.

4. Nitrogen-Doped Graphene for Photocatalytic H₂ Generation

4.1. Composite photocatalyst with metal oxides and nitrogen-doped graphene

Since the first report on a photocatalytic water splitting process with TiO₂,^[2a] various metal oxides have been intensively employed as a semiconducting photocatalyst. High efficiency in the photocatalytic water splitting process in diverse conditions has been achieved by metal oxide catalysts.^[5a] Specifically, TiO₂ possesses several additional advantages such as high photostability, low cost, easy processability, and environmental friendliness. However, undesirable rapid recombination of photo-induced electron–hole pairs as well as backward reaction can easily occur in pristine TiO₂. Furthermore, the wide band gap of TiO₂ allows it to interact mainly with UV light, which can limit the use of the total solar energy. To solve these problems, multi-component composite formation of TiO₂ with metals,^[29] heteroatoms,^[30] semiconductors^[5a] and CNTs^[31] has been developed. Notably, nitrogen-doped graphene with incorporation of TiO₂ and other semiconductors is expected to show potential as a photocatalyst, because it can not only supply nucleation and/or anchoring sites for metal oxides but

also imparts several advantages such as reduced photo-induced charge recombination through fast transportation of photo-induced charges and improved visible-light absorption to a newly formed composite photocatalyst.

Mou et al. fabricated TiO₂ nanoparticle-functionalized nitrogen-doped graphene (NGR) composites (NGR/TiO₂) by a solvothermal treatment for photocatalytic hydrogen generation for water (Figure 5).^[11d] NGR showed better electrical conductivity than conventional reduced graphene oxide (RGO), due to efficient structural restoration and smaller populations of defects in the graphitic structure. Interestingly, it was found that nitrogen atoms in NGR play important roles as nucleation and anchor sites for TiO₂ nanoparticles on NGR, resulting in close interfacial contact between TiO₂ nanoparticles and NGR, and a uniform distribution of them on the graphene sheet. The photocatalytic activities for H₂ production were assessed under a 150 W xenon lamp in the presence of triethanolamine (TEOA) as a sacrificial agent. The average rate of H₂ production of NGR/TiO₂ can reach 13.3 μmol h⁻¹, which is higher than that of RGO/TiO₂ (8.9 μmol h⁻¹).^[11d] In addition, improved durability during the photocatalytic process was observed from NGR/TiO₂. These results clearly reveal the huge potential of nitrogen-doped graphene in TiO₂-based composite photocatalysts.

Pei et al. also reported an effective improvement of photocatalytic hydrogen evolution by using nanocomposite catalysts (NTNG) composed of nitrogen-doped TiO₂ (N-TiO₂) and nitrogen-doped graphene (NG).^[11e] In this study, NTNG was prepared by a conventional in-situ solvothermal nitrogen-doping

process with TiO₂ and NG in the presence of 1,2-diaminoethane as a nitrogen source. Owing to the existence of numerous bridges such as Ti–O–C and Ti–C, uniform dispersion of N-TiO₂ nanoparticles in NTNG was observed. Simultaneously, the wrinkled multi-layer textures of pristine NG were significantly stretched after the formation of NTNG. Apart from these morphological changes, several structural changes in NTNG also took place during the solvothermal nitrogen-doping process, which includes nitrogen doping and nitrogen re-doping of TiO₂ and NG, respectively, as well as structural restoration of graphitic structures by enhancement of sp²-hybridized nitrogen content in NG through the cyclic substitution of chlorine atoms and dehydrogenation reactions (Figure 6a). As shown in Figure 6b, the band gap was greatly altered by nitrogen-doping. The calculated band gaps of TiO₂, N-TiO₂, and NTNG were 3.25, 2.90, and 2.78 eV, respectively, and the lower band gap of NTNG was beneficial for efficient absorption of solar light. The photocatalytic properties of all materials were measured under irradiation of a 500 W high-pressure Hg lamp with methanol as a sacrificial agent. The amount of hydrogen evolution of TiO₂, N-TiO₂, and NTNG was 76.1, 270.0, and 996.8 μmol h⁻¹ g⁻¹, respectively (Figure 6c). As illustrated in Figure 6d, this significant improvement in the photocatalytic efficiency of NTNG may be caused by several factors including efficient charge generation on N-TiO₂, fast transportation of photo-generated charges, and facile reduction of H⁺ on the active position of NTNG. As a result, an appropriate combination of nitrogen-doped graphene with N-TiO₂ can be regarded as a promising tool to construct a high-performance catalyst for photocatalytic H₂ generation.

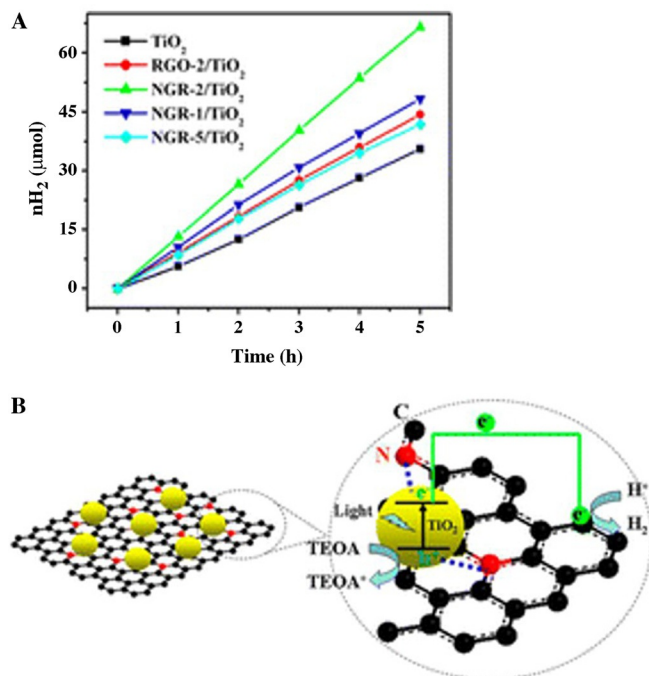


Figure 5. A) Time course of hydrogen production from a 50 mL aqueous solution containing 10 vol% TEOA aqueous solution with different catalysts. B) Schematic illustration of the strong coupling between TiO₂ and N atoms in the NGR sheet and enhanced photo-induced charge transfer and photocatalytic hydrogen generation. Adapted from Ref. [11d] with permission, American Chemical Society.

4.2. Composite photocatalysts with metal sulfide and nitrogen-doped graphene

In addition to metal oxides, some other compounds such as metal sulfides (e.g., CdS, ZnS, and MoS) also have been developed as catalysts or co-catalysts for photocatalytic H₂ generation due to their unique electronic and catalytic properties.^[5a] However, metal sulfides are highly susceptible to photo-corrosion under irradiation of sunlight. For example, the photo-induced holes in the valence band of CdS can usually oxidize S²⁻ in CdS rather than water, as shown in the equation of CdS + 2h⁺ → Cd²⁺ + S.

Interestingly, Jia et al. developed a series of nitrogen-doped graphene (N-graphene)/CdS nanocomposites for photocatalytic H₂ generation under visible-light irradiation.^[11a] Different content of N-graphene ranging from 0.5 to 5 wt% was loaded to nanocomposites by controlled experiments. Owing to intimate contact between N-graphene and CdS nanoparticles, the uniform dispersion of CdS nanoparticles on N-graphene and wide absorption in the visible-light region was clearly observed from nanocomposites. The photocatalytic H₂ generation properties of nanocomposites were measured under visible-light irradiation (λ ≥ 420 nm) with NaS-Na₂SO₃ as sacrificial donors. Although N-graphene alone did not produce any H₂, the photocatalytic activities were significantly enhanced by N-graphene/CdS nanocomposite even compared with a solitary CdS photo-

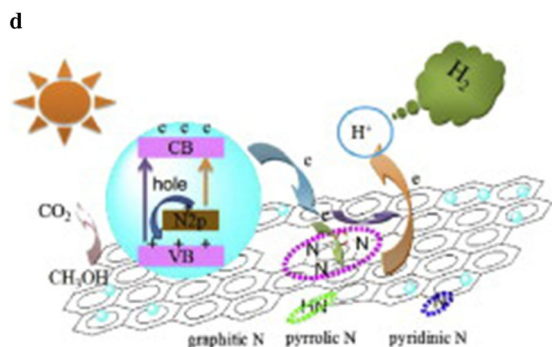
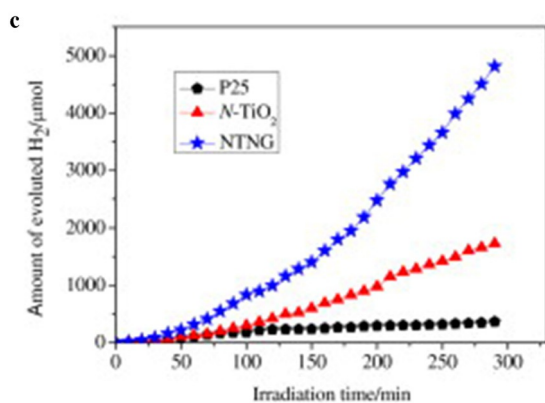
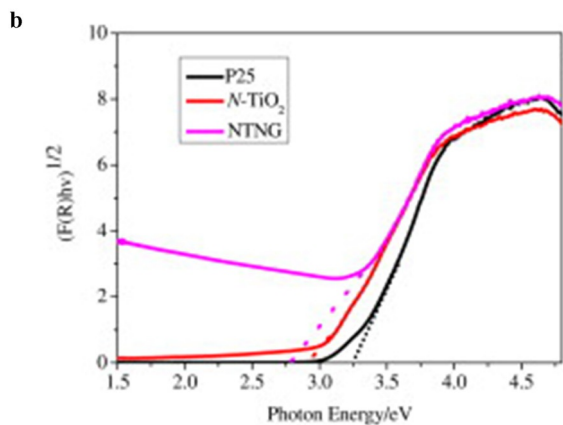
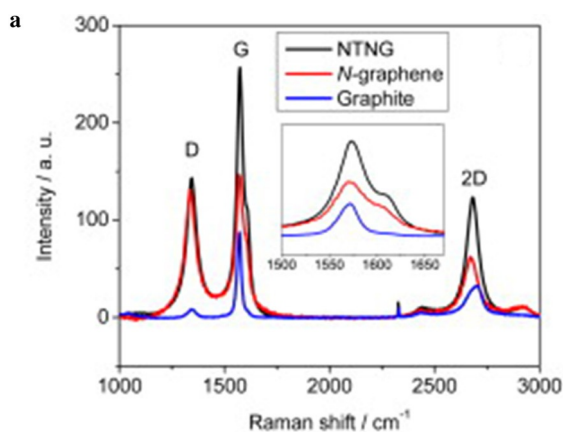


Figure 6. A) Enlarged Raman spectra of pristine graphite, NG, and NTNG. B) Corresponding plot of the transformed Kublika–Munk function vs. photon energy. C) Amount of H₂ produced as a function of time. D) Proposed schematic illustration of the mechanism of the photocatalytic H₂ generation process on NTNG photocatalyst. Adapted from Ref. [11e] with permission, Elsevier.

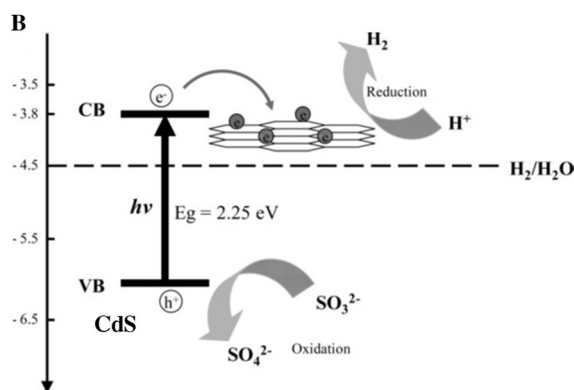
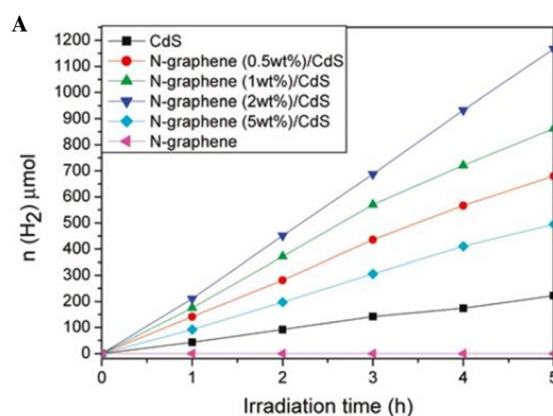


Figure 7. A) H₂ evolution of various photocatalysts used in this study. B) The energy level diagram for N-graphene/CdS nanocomposite. Adapted from Ref. [11a] with permission, American Chemical Society.

catalyst (Figure 7A). It was also found that the optimum amount of N-graphene is approximately 2 wt%, at which the nanocomposite photocatalyst showed the highest H₂ evolution rate of 210 μmol h⁻¹. The higher content of N-graphene in the nanocomposite could increase the opacity and light scattering of the reaction solution, which led to a decrease of light absorption during the photocatalytic H₂ generation process. The enhancement of the photocatalytic activity of nanocomposites could be attributed to an effective retardation of electron–hole recombination through facile photo-induced electron transfer from the valence band of CdS to N-graphene. As shown in Figure 7B, the electron transfer from CdS to N-graphene is energetically favorable because the conducting band of CdS (−3.8 eV) is smaller than the work function of graphene (−4.4 eV). Furthermore, the nanocomposite photocatalysts did not exhibit a noticeable decrease in photocatalytic activity for prolonged reaction times up to 30 h, which reveals that the incorporation of N-graphene into CdS can greatly improve the photostability of CdS. The photocorrosion of the pristine CdS catalyst usually starts after an irradiation time of over 4 h.^[32] These results clearly show the remarkable potential of N-graphene in composite photocatalysts with metal sulfides as an electron-transporting and a protective layer.

Meng et al. also reported solar hydrogen generation using a photocatalyst containing a nanoscale p–n junction between p-type molybdenum disulfide (MoS₂) and n-type nitrogen-

doped reduced graphene oxide (n-rGO).^[11c] Although MoS₂ possesses characteristics suitable for a photocatalyst including a longer absorption band reaching 1040 nm, non-toxicity, and cost-effectiveness, the insufficient photo-induced charge separation and transportation in MoS₂ render it almost inactive as a photocatalyst.^[33] However, it has been found that the combination of a ruthenium-based photosensitizer with MoS₂ can produce noticeable photocatalytic activity, which has opened new strategies for the development of a MoS₂-based photocatalyst.^[34] In this regard, a p-type thin nanoplatelet MoS₂ structure was deposited on n-type n-rGO using a hydrothermal process to introduce a useful p-n heterojunction (see above). The nanoplatelet geometry of MoS₂ was designed for enlarging the contact area with the n-rGO sheet and lowering the recombination loss during volume diffusion. The newly formed nano-scale p-n heterojunction between MoS₂ and n-rGO could not only enhance the photo-induced charge generation but also inhibit the undesirable recombination of electron-hole pairs (Figure 8A). The photocatalytic H₂ generation measurement of the sample was conducted with a 300 W Xenon lamp solar simulator, and ethanol was used as a hole-scavenging sacrificial reagent. For a comparative study, three types of photocatalysts, pristine MoS₂, MoS₂ on reduced graphene (MoS₂/rGO), and MoS₂ on n-rGO (MoS₂/n-rGO) were tested, and the results are shown in Figure 8B. As expected, pristine MoS₂ exhibited almost negligible H₂ generation (0.1 μmol h⁻¹ g⁻¹). However, evident photocatalytic activity has been observed (7.4 μmol h⁻¹ g⁻¹) when MoS₂ was supported on the undoped rGO (MoS₂/rGO). Interestingly, MoS₂/n-rGO shows a dramatically

enhanced photocatalytic activity and the hydrogen generation rate can reach 24.8 μmol h⁻¹ g⁻¹. These results, with further analyses of electronic properties of MoS₂/n-rGO, clearly reveal that n-rGO is an active component of the photocatalyst to form a p-n heterojunction and is highly beneficial for improving the photocatalytic performance by enhancing three critical processes of photocatalysis, that is, charge separation, migration, and recombination.

Maitra et al. also reported highly effective visible-light-induced H₂ generation using a nanocomposite photocatalyst of few-layer 2H-MoS₂ with heavily nitrogen-doped graphene (NRGO).^[11b] As a polytype of MoS₂, 2H-MoS₂ is a semiconductor with an indirect band gap of 1.2 eV, while 1T-MoS₂ is metallic.^[35] 1T-MoS₂ is metastable and thus can readily undergo transition to the more stable 2H-MoS₂ with time. The photocatalytic activities of the nanocomposite with 2H-MoS₂ and NRGO (NRGO-2H-MoS₂) were investigated in the presence of eosin-Y (EY) and triethanolamine (TEOA) as a photosensitizer and sacrificial agent, respectively. Under these conditions, photo-induced electrons responsible for the reduction of H₂O to produce H₂ were first generated by EY sensitizers. They were then transported and collected to n-type NRGO and finally reached a p-type 2H-MoS₂ semiconductor. The overall mechanism of photocatalytic H₂ generation using NRGO-2H-MoS₂ photocatalyst is shown in Figure 9A. Therefore, NRGO can play important roles as an electron channel between the photosensitizer and semiconductor, which is favorable to enhance photocatalytic H₂ generation. Compared with a catalyst using an undoped graphene (RGO) support, the NRGO-based catalyst showed a re-

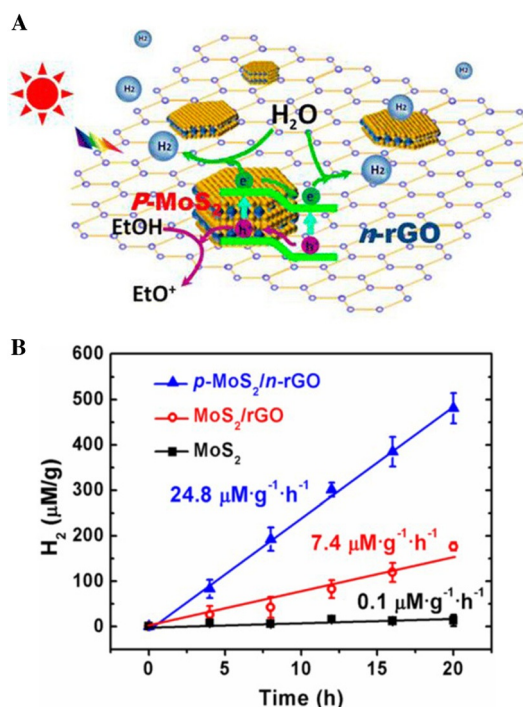


Figure 8. A) Schematic illustration of the photocatalytic H₂ generation process with MoS₂/n-rGO. B) Hydrogen generated by the MoS₂, MoS₂/rGO and MoS₂/n-rGO photocatalysts. Adapted from Ref. [11c] with permission, American Chemical Society.

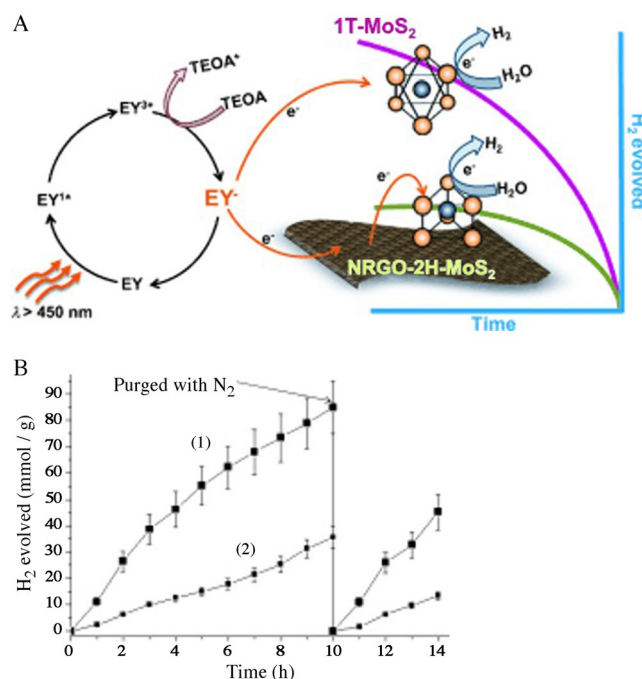


Figure 9. A) Schematic illustration of the photocatalytic H₂ generation process with a few-layer nanocomposite of 2H-MoS₂ with heavily nitrogenated graphene. B) Time course of H₂ evolution by (1) NRGO-MoS₂ and (2) RGO-MoS₂ per gram of catalyst. After 10 h of H₂ evolution, the vessel was purged with N₂. Adapted from Ref. [11b] with permission, Wiley-VCH.

markedly enhanced photocatalytic activity originating from the facile electron transfer through existing p-n heterojunctions between n-type NRGO and p-type 2H-MoS₂. A higher yield of H₂ evolution (10.8 mmol h⁻¹ g⁻¹) was obtained from NRGO-2H-MoS₂ compared to that from RGO-2H-MoS₂ (3.0 mmol h⁻¹ g⁻¹) (Figure 9B). Interestingly, metallic 1T-MoS₂ showed more profound photocatalytic activities than NRGO-2H-MoS₂, which implies the importance of conductivity of the photocatalyst for photocatalytic H₂ generation. Therefore, NRGO can be regarded as a promising constituent in photocatalysts due to its unique electron-accepting and -transporting properties.

4.3. Nitrogen-doped graphene as photocatalysts

To date, various composite photocatalysts with nitrogen-doped graphene as a support matrix have been explored. In these configurations, other semiconducting components are additionally required to obtain meaningful photocatalytic activities toward H₂ generation. The role of nitrogen-doped graphene in the photocatalyst has also some limitations such as serving as anchoring sites and/or auxiliary channels for photo-induced charge separation and migration. However, since the report on the noticeable photocatalytic activity of graphene oxide (GO) itself after band gap modulation, considerable attention has been devoted to utilizing graphene as a sole photocatalyst.^[36]

Recently, Yeh et al. developed nitrogen-doped graphene oxide quantum dots (NGO-QDs) as a photocatalyst for the overall water-splitting process under visible-light illumination.^[12b] NGO-QDs were synthesized by treating GO with NH₃ at 500 °C followed by a harsh oxidation step using a modified Hummer's method. As shown in Figure 10A, panels a and b, the particle size of NGO-QDs was calculated as 8.1 ± 1.8 nm with visible crystalline lattice fringes with an interlayer spacing of 0.213 nm. Various sized single crystalline graphene layers were intimately stacked in AB order (Figure 10A, panels c–e). Nitrogen atoms in the basal plane and oxygenated functional groups at the edge of NGO-QDs could be successfully introduced during high-temperature NH₃ treatment and a subsequent oxidation process, respectively (Figure 10A, panel f). The co-doping of nitrogen and oxygen atoms in the graphitic structure could provide inherent n- and p-type conductivities to NGO-QDs at the same time. The conduction band (CB) and valence band (VB) of NGO-QDs were estimated as -0.85 and 1.35 eV (vs. Ag/AgCl), respectively. The location of CB and VB together with a small band gap of 2.2 eV was estimated to be favorable for the overall water splitting process including water oxidation (O₂/H₂O) and hydrogen reduction (H⁺/H₂).^[12b] In addition, the presence of small sp² clusters at the interfacial junction, in which most of the photo-induced charge carriers are recombined to produce useful electron-hole pairs, has been proven by the strong photoluminescence (PL) spectra of

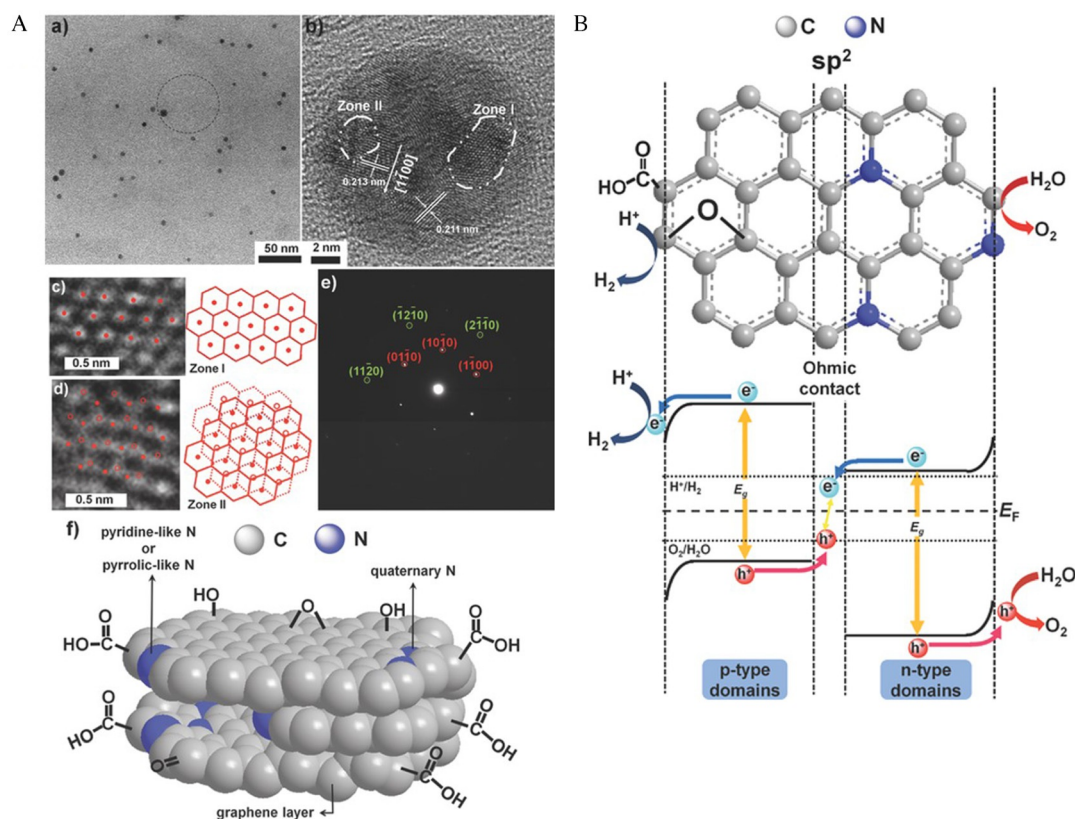


Figure 10. A) Morphological and crystal structure of NGO-QDs. a) TEM image of NGO-QDs, b–d) high-resolution TEM image of various areas in NGO-QDs, e) the selected-area electron diffraction pattern of NGO-QDs, f) a conceptual structure of NGO-QDs. B) The configuration of the energy diagram for the NGO-QD photochemical diode for the photocatalytic water splitting process. Adapted from Ref. [12b] with permission, Wiley-VCH.

NGO-QDs under visible-light irradiation. Therefore, the typical diode system consisting of p- and n-domains linked to the sp^2 clusters as ohmic contact could be created in NGO-QDs (Figure 10B). P-type domains and n-type domains in NGO-QDs are responsible for electron injection for H_2 evolution and hole injection for O_2 generation, respectively. As a result, the irradiation of visible light ($420\text{ nm} < \lambda < 800\text{ nm}$) on the dispersion of NGO-QDs in pure water could efficiently produce H_2 and O_2 with a molar ratio of 2:1 with good operational stability. The observed overall water splitting process on NGO-QDs is quite similar to biological photosynthesis. In addition, a synergistic effect of oxygen and nitrogen functionalities in nitrogen-doped graphene quantum dots (iNGO-QDs) for photocatalytic H_2 production from water decomposition was also reported.^[12c] These results clearly demonstrate the huge potential of nitrogen-doped graphene as metal-free, cost-effective, and environmentally friendly catalyst for the photocatalytic water splitting process.

Lavorato et al. also reported the use of nitrogen-doped graphene (NG) as a visible-light photocatalyst for photocatalytic H_2 generation.^[12a] In this study, NG was prepared by pyrolysis of chitosan at high temperature (Figure 11A). As a natural nitrogen-containing biopolymer, chitosan could be used as a single source of carbon and nitrogen, making the nitrogen-doping process in the graphitic structure more straightforward. All samples showed typical characteristics of graphene as well as a high amount of nitrogen content in their structures, which clearly demonstrate the successful transformation of chitosan to NG. It was found that the nitrogen content in NG decreased with increasing pyrolysis temperature. The highest weight percentage of nitrogen (16.2%) was observed in NG-200, while NG-900 showed the lowest weight percentage of nitrogen (5.4%). The numbers in the sample correspond to the pyrolysis temperature. As shown in Figure 11B, all NG samples synthesized at various pyrolysis temperatures in the range of

200 and 900 °C exhibited noticeable photocatalytic H_2 generation properties under irradiation of UV light at 355 nm. In the photocatalytic reaction solution, methanol was added to the reaction solution to provide sacrificial electron donors. The highest evolution of H_2 has been observed in the sample prepared at 900 °C (NG-900), outperforming other NGs obtained from lower pyrolysis temperature. These results could be attributed to the greater dependence of the photocatalytic activity of NGs on the structural restoration of graphitic structures with reduced defects than on the content of nitrogen atoms in NG. In addition, NG-900 exhibited similar photocatalytic activity under irradiation of simulated solar-light irradiation (Figure 11C).

5. Other Heteroatom-Doped Graphenes for Photocatalytic H_2 Generation

Apart from the incorporation of n-type nitrogen atoms, chemical doping of graphene structures with other heteroatoms such as boron (B) and phosphorous (P), which results in p-type conductive behaviors, can be simultaneously considered for the preparation of a graphene-based photocatalyst. As noticed on nitrogen-doped graphene, numerous advantages in photocatalytic activities including band gap tuning to semiconductors, the generation of active sites with high populations, and improvement of charge transport properties also can be expected from boron- or phosphorous-doped graphene.^[37] Very recently, Xiang et al. reported the utilization of boron-doped graphene as a photodegradation of rhodamine B (RhB),^[38] and Ran et al. also reported the fabrication of porous phosphorous-doped graphitic carbon nitride ($g\text{-}C_3N_4$) for visible-light photocatalytic H_2 production with an apparent quantum efficiency.^[39] These results clearly demonstrate the high potential of p-type doping in graphitic structures for photocatalysts.

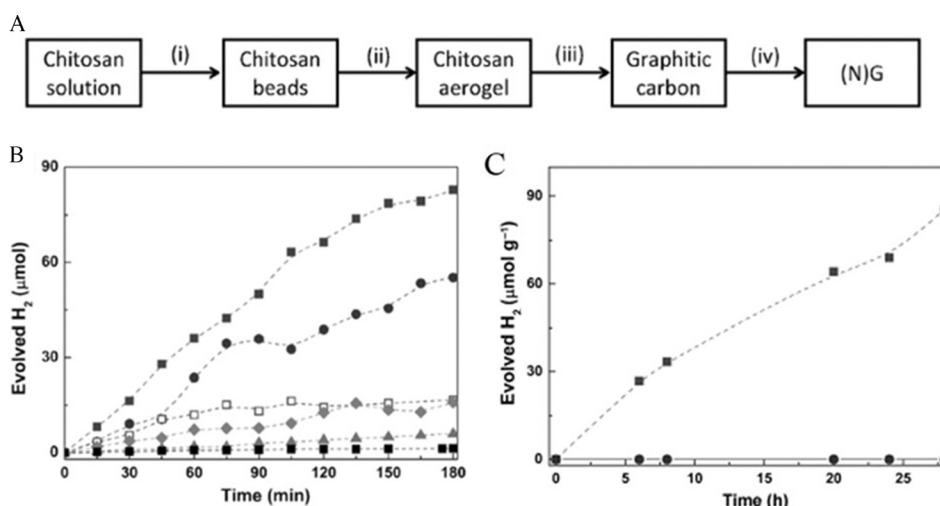


Figure 11. A) Synthesis of NG. i) Formation of a chitosan hydrogel; ii) formation of a chitosan aerogel; iii) pyrolysis of the chitosan aerogel; iv) exfoliation in water by ultrasonication. B) Hydrogen evolution upon 355 nm irradiation of a water/methanol mixture in the presence of NG obtained from chitosan pyrolysis at different temperatures (■: GO; ▲: NG-200; ◆: NG-400; □: NG-600; ●: NG-800; ■: NG-900). C) Hydrogen evolution under irradiation of simulated solar light (■: NG-900; ●: GO). Adapted from Ref. [12a] with permission, Wiley-VCH.

Sanchez et al. reported that phosphorous-doped graphene (PG) exhibits significant photocatalytic activity for H₂ generation from a water-methanol mixture.^[40] PG was synthesized by pyrolysis of phosphorous-containing alginate at 900 °C under an inert atmosphere (Figure 12A). Alginate is a natural anionic polymer from seaweed and regarded as a non-toxic, low-cost, and biocompatible material.^[41] Prior to pyrolysis, alginate was modified with various amounts of H₂PO₄⁻ in an aqueous solution at neutral pH, in which H₂PO₄⁻ was used as a phosphorous resource during pyrolysis at high temperature. Further structural analyses of PG clearly exhibited the successful formation of phosphorous-doped graphene networks. The photocatalytic activities of PG were measured by irradiation of UV/Vis light using a Xe lamp in the presence of methanol as a sacrificial donor, and the results are summarized in Figure 12B. The graphene (G) obtained by pyrolysis of pristine alginate, reduced graphene oxide (rG), and graphene oxide (GO) showed almost negligible activity for photocatalytic H₂ generation. However, the rate of H₂ evolution was greatly improved with increasing phosphorous content in PG, and the highest catalytic activity was obtained from PG-4, which showed the lowest C/P atomic ratio of 12.73. By changing light sources during experiments, it was found that a large percentage of photocatalytic H₂ generation by PG was derived from UV light excitation. In addition, the incorporation of platinum (Pt) nanoparticles on PG-4 could greatly improve the rate of H₂ evolution in the presence of TEOA (Figure 12C). Although meaningful catalytic properties for photocatalytic H₂ generation were obtained with phospho-

rus-doped graphene (PG) used in this study, the research on p-type graphene photocatalysts is still in its infancy. More efforts should be devoted to the development of high-performance heteroatom-doped photocatalysts for H₂ evolution with enhanced activity in the visible range, cost effectiveness, environmental friendliness, and long-term stability.

6. Conclusions and Perspectives

In this review, recent developments related to nitrogen-doped graphene for photocatalytic H₂ generation have been discussed, and some noticeable achievements are summarized in Table 1. Owing to its unique properties and versatilities, nitrogen-doped graphene has rapidly emerged as a new photocatalyst with diverse functions including photo-induced charge acceptor/mediator, a light absorber from UV to visible light, an n-type semiconductor, and a giant molecular photocatalyst. The outstanding potential of nitrogen-doped graphene has been demonstrated by the high efficiency of photocatalytic H₂ evolution with additional advantages of cost effectiveness, environmental friendliness, and photostability.

In spite of this remarkable progress, the research in this field is still in its infancy. Many additional challenges remain for the employment of nitrogen-doped graphene as a photocatalyst in photocatalytic H₂ generation. First, the synthesis of high-quality nitrogen-doped graphene with a controlled morphology and tailored electronic properties is important because the performance of the photocatalyst is closely related to the in-

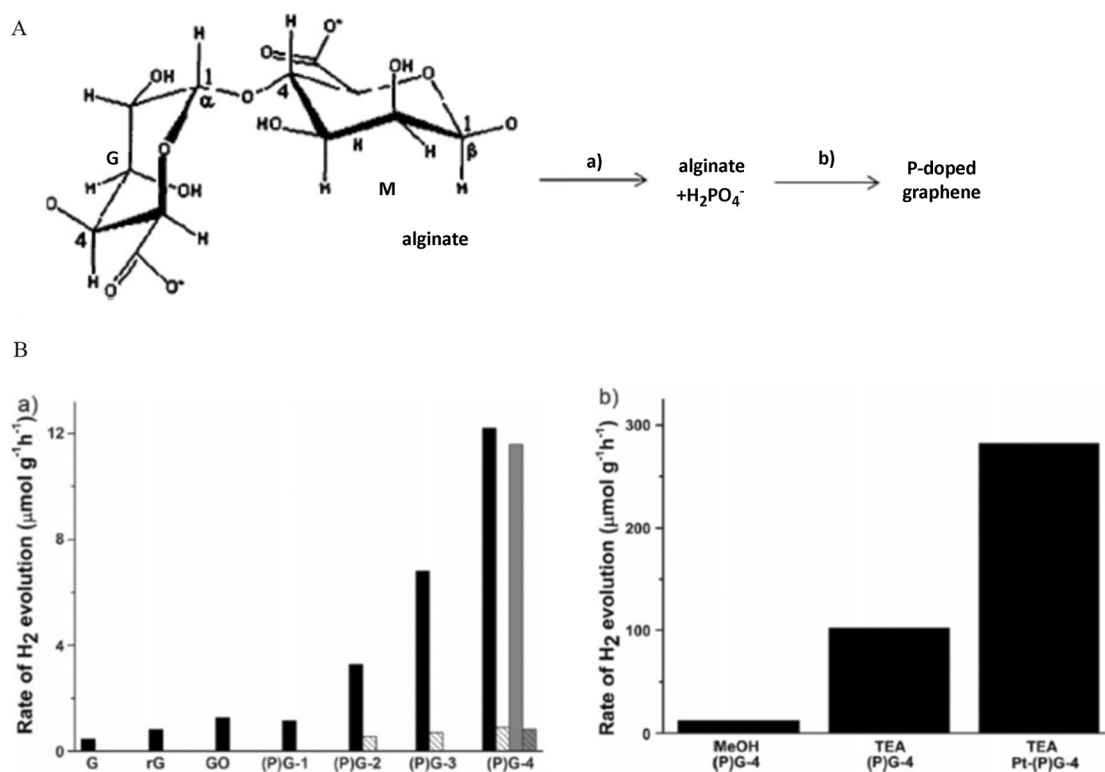


Figure 12. A) Preparation of PG. a) Addition of H₂PO₄⁻ and (b) pyrolysis of phosphate-containing alginate at 900 °C. B) a) Photocatalytic activity for H₂ generation of various samples, black: UV/Vis, shaded white: visible light, gray: UV/Vis and third use of catalyst, shaded gray: visible light and third use of catalyst, b) the H₂ production rate of PG-4 in methanol and TEOA, and for Pt-PG-4 in TEA under UV/Vis irradiation. Adapted from Ref. [40] with permission, Wiley-VCH.

Table 1. Summary of nitrogen-doped graphene for photocatalytic H₂ generation.

Types of photocatalysts	Role of n-doped graphene (preparation method of photocatalyst)	Light source	H ₂ production	Remarks	Ref.
Composites of TiO ₂ /N-doped graphene (10 at. % N)	Supporting matrix (hydrothermal reaction)	150 W Xenon lamp	13.3 μmol h ⁻¹	Efficient charge transport and separation	[11d]
Composites of N-TiO ₂ /N-doped graphene (3.5 at. % N)	Supporting matrix (solvochemical reaction)	500 W high pressure Hg lamp	996.8 μmol h ⁻¹ g ⁻¹	Improved absorption, charge generation and transportation	[11e]
Composites of CdS/N-doped graphene (4.3 at. % N)	Supporting matrix (wet chemical reaction and thermal annealing at high temperature)	300 W Xenon lamp (λ ≥ 420 nm)	210 μmol h ⁻¹	N-doped graphene as an electron transfer channel	[11a]
Composites of MoS ₂ /N-doped graphene (6.4 at. % N)	Supporting matrix (hydrothermal reaction and post nitrogen doping with ammonia gas)	300 W Xenon lamp with an AM1.5G filter	24.8 μmol h ⁻¹ g ⁻¹	Enhanced contact area and formation of nanoscale p-n junction	[11c]
Composites of 2H-MoS ₂ /N-doped graphene (15 at. % N)	Supporting matrix (hydrothermal reaction)	300 W halogen lamp	10.8 mmol h ⁻¹ g ⁻¹	Formation of p-n junction and efficient electron transport	[11b]
N-doped graphene quantum dots (atomic ratio of N/C = 2.9%)	Direct photocatalyst (treating GO in NH ₃ at 500 °C and then harsh oxidation)	300 W Xenon lamp with UV- and IR-cutoff filter	Approx. 0.57 μmol h ⁻¹	Metal-free, cost-effective and environmental friendly photocatalyst with p-n junction	[12b]
N-doped graphene (N content 5.4 ~ 16.2 wt %)	Direct photocatalyst (pyrolysis of chitosan aerogel)	1000 W solar simulator	Approx. 4 μmol h ⁻¹ g ⁻¹	N-doped graphene semiconductor	[12a]

intrinsic nature of nitrogen-doped graphene, such as its band-gap, structural integrity, functionality, and so on. From this point of view, recently developed edge-selectively functionalized graphene (EFG) via either a mechano-chemical ball-milling process or direct Friedel–Crafts acylation reaction can be regarded as a promising candidate for preparing nitrogen-doped graphene for photocatalytic H₂ generation. The unique structural configuration of EFG, with minimal damage to the basal plane and high populations of functional groups on edges, is expected to be highly beneficial to the photocatalyst. Second, the simultaneous chemical doping of p-type boron (B) or phosphorous (P) as well as n-type nitrogen (N) to produce co-doped graphene could be an important step in the development of high-performance photocatalysts because countless atomic-scale p-n heterojunctions within graphene networks can be directly formed. For example, a remarkable enhancement of electrocatalytic activity for ORR has been obtained from BCN graphene, in which both B and N atoms are co-doped at the same time.^[42] Finally, the incorporation of photosensitizers into nitrogen-doped graphene through physical adsorption or chemical linkage can also be considered a meaningful approach.^[43] This hybrid photocatalyst system can improve not only solar light absorption but also photo-induced charge generation and separation through intimate contact between two materials. Although three plausible approaches have been proposed here, it is believed that there is still much room for further improvement of the photocatalytic activity of nitrogen-doped graphene. In addition, with ongoing and innovative efforts, nitrogen-doped graphene is a promising catalyst for photocatalytic H₂ generation.

Acknowledgements

This research work was supported by the Basic Science Research (2013R1A1A2007716), Creative Research Initiative (CRI) and BK21 Plus programs through the National Research Foundation (NRF) of Korea funded by the Ministry of Education, Science and Technology (MEST) and UNIST.

Keywords: nitrogen-doped graphene · photocatalysts · photocatalytic hydrogen generation · semiconductors · water splitting

- [1] a) C. W. Tang, *Appl. Phys. Lett.* **1986**, *48*, 183–185; b) B. O'Regan, M. Grätzel, *Nature* **1991**, *353*, 737–740.
- [2] a) A. Fujishima, K. Honda, *Nature* **1972**, *238*, 37–38; b) T. Inoue, A. Fujishima, S. Konishi, K. Honda, *Nature* **1979**, *277*, 637–638.
- [3] H. Ahmad, S. Kamarudin, L. Minggu, M. Kassim, *Renewable Sustainable Energy Rev.* **2015**, *43*, 599–610.
- [4] a) L. S. Al-Mazroai, M. Bowker, P. Davies, A. Dickinson, J. Greaves, D. James, L. Millard, *Catal. Today* **2007**, *122*, 46–50; b) G. L. Chiarello, M. H. Aguirre, E. Selli, *J. Catal.* **2010**, *273*, 182–190.
- [5] a) X. Chen, S. Shen, L. Guo, S. S. Mao, *Chem. Rev.* **2010**, *110*, 6503–6570; b) J. Ran, J. Zhang, J. Yu, M. Jaroniec, S. Z. Qiao, *Chem. Soc. Rev.* **2014**, *43*, 7787–7812.
- [6] a) M. J. Allen, V. C. Tung, R. B. Kaner, *Chem. Rev.* **2010**, *110*, 132–145; b) A. K. Geim, K. S. Novoselov, *Nat. Mater.* **2007**, *6*, 183–191; c) K. Novoselov, A. Geim, S. Morozov, D. Jiang, Y. Zhang, S. Dubonos, I. Grigorieva, A. Firsov, *Science* **2004**, *306*, 666–669.
- [7] a) L. Dai, D. W. Chang, J. B. Baek, W. Lu, *Small* **2012**, *8*, 1130–1166; b) Y. Sun, Q. Wu, G. Shi, *Energy Environ. Sci.* **2011**, *4*, 1113–1132.
- [8] a) X. K. Kong, C.-L. Chen, Q. W. Chen, *Chem. Soc. Rev.* **2014**, *43*, 2841–2857; b) K. P. Loh, Q. Bao, P. K. Ang, J. Yang, *J. Mater. Chem.* **2010**, *20*, 2277–2289.

- [9] a) L. Dai, Y. Xue, L. Qu, H. J. Choi, J. B. Baek, *Chem. Rev.* **2015**, *115*, 4823–4892; b) H. Wang, T. Maiyalagan, X. Wang, *ACS Catal.* **2012**, *2*, 781–794.
- [10] a) L. K. Putri, W. J. Ong, W. S. Chang, S. P. Chai, *Appl. Surf. Sci.* **2015**, *358*, 2–14; b) Q. Xiang, B. Cheng, J. Yu, *Angew. Chem. Int. Ed.* **2015**, *54*, 11350–11366; *Angew. Chem.* **2015**, *127*, 11508–11524; c) N. Zhang, M. Q. Yang, S. Liu, Y. Sun, Y. J. Xu, *Chem. Rev.* **2015**, *115*, 10307–10377.
- [11] a) L. Jia, D. H. Wang, Y. X. Huang, A. W. Xu, H. Q. Yu, *J. Phys. Chem. C* **2011**, *115*, 11466–11473; b) U. Maitra, U. Gupta, M. De, R. Datta, A. Govindaraj, C. Rao, *Angew. Chem. Int. Ed.* **2013**, *52*, 13057–13061; *Angew. Chem.* **2013**, *125*, 13295–13299; c) F. Meng, J. Li, S. K. Cushing, M. Zhi, N. Wu, *J. Am. Chem. Soc.* **2013**, *135*, 10286–10289; d) Z. Mou, Y. Wu, J. Sun, P. Yang, Y. Du, C. Lu, *ACS Appl. Mater. Interfaces* **2014**, *6*, 13798–13806; e) F. Pei, S. Xu, W. Zuo, Z. Zhang, Y. Liu, S. Cao, *Int. J. Hydrogen Energy* **2014**, *39*, 6845–6852.
- [12] a) C. Lavorato, A. Primo, R. Molinari, H. Garcia, *Chem. Eur. J.* **2014**, *20*, 187–194; b) T. F. Yeh, C. Y. Teng, S. J. Chen, H. Teng, *Adv. Mater.* **2014**, *26*, 3297–3303; c) T. F. Yeh, S. J. Chen, H. Teng, *Nano Energy* **2015**, *12*, 476–485.
- [13] a) E. Bundgaard, F. C. Krebs, *Sol. Energy Mater. Sol. Cells* **2007**, *91*, 954–985; b) B. Kippelen, J. L. Brédas, *Energy Environ. Sci.* **2009**, *2*, 251–261.
- [14] J. S. Jang, H. G. Kim, J. S. Lee, *Catal. Today* **2012**, *185*, 270–277.
- [15] H. Li, Z. Bian, J. Zhu, Y. Huo, H. Li, Y. Lu, *J. Am. Chem. Soc.* **2007**, *129*, 4538–4539.
- [16] J. Wang, D. N. Tafen, J. P. Lewis, Z. Hong, A. Manivannan, M. Zhi, M. Li, N. Wu, *J. Am. Chem. Soc.* **2009**, *131*, 12290–12297.
- [17] a) D. Li, H. Haneda, *Chemosphere* **2003**, *51*, 129–137; b) Z. Wu, F. Dong, W. Zhao, H. Wang, Y. Liu, B. Guan, *Nanotechnology* **2009**, *20*, 235701.
- [18] a) A. Nozik, *Appl. Phys. Lett.* **1976**, *29*, 150–153; b) O. Khaselev, J. A. Turner, *Science* **1998**, *280*, 425–427.
- [19] N. Zhang, Y. Zhang, M. Q. Yang, Z. R. Tang, Y.-J. Xu, *J. Catal.* **2013**, *299*, 210–221.
- [20] L. Qu, Y. Liu, J. B. Baek, L. Dai, *ACS Nano* **2010**, *4*, 1321–1326.
- [21] a) P. Chen, J. J. Yang, S.-S. Li, Z. Wang, T. Y. Xiao, Y. H. Qian, S. H. Yu, *Nano Energy* **2013**, *2*, 249–256; b) J. Wu, D. Zhang, Y. Wang, B. Hou, *J. Power Sources* **2013**, *227*, 185–190.
- [22] a) Z. H. Sheng, L. Shao, J. J. Chen, W. J. Bao, F. B. Wang, X. H. Xia, *ACS Nano* **2011**, *5*, 4350–4358; b) Y. Shao, S. Zhang, M. H. Engelhard, G. Li, G. Shao, Y. Wang, J. Liu, I. A. Aksay, Y. Lin, *J. Mater. Chem.* **2010**, *20*, 7491–7496.
- [23] E. J. Biddinger, D. Von Deak, U. S. Ozkan, *Top. Catal.* **2009**, *52*, 1566–1574.
- [24] D. Geng, Y. Chen, Y. Chen, Y. Li, R. Li, X. Sun, S. Ye, S. Knights, *Energy Environ. Sci.* **2011**, *4*, 760–764.
- [25] a) Z. Luo, S. Lim, Z. Tian, J. Shang, L. Lai, B. MacDonald, C. Fu, Z. Shen, T. Yu, J. Lin, *J. Mater. Chem.* **2011**, *21*, 8038–8044; b) D. W. Chang, H. J. Choi, J. B. Baek, *J. Mater. Chem. A* **2015**, *3*, 7659–7665.
- [26] D. W. Chang, H. J. Choi, I. Y. Jeon, J. B. Baek, *Chem. Rec.* **2013**, *13*, 224–238.
- [27] I. Y. Jeon, D. Yu, S. Y. Bae, H. J. Choi, D. W. Chang, L. Dai, J. B. Baek, *Chem. Mater.* **2011**, *23*, 3987–3992.
- [28] I. Y. Jeon, H. J. Choi, M. J. Ju, I. T. Choi, K. Lim, J. Ko, H. K. Kim, J. C. Kim, J. J. Lee, D. Shin, *Sci. Rep.* **2013**, *3*, 1–7.
- [29] A. A. Ismail, *Appl. Catal. B* **2012**, *117*, 67–72.
- [30] R. Asahi, T. Morikawa, H. Irie, T. Ohwaki, *Chem. Rev.* **2014**, *114*, 9824–9852.
- [31] H. Park, Y. Park, W. Kim, W. Choi, *J. Photochem. Photobiol. C* **2013**, *15*, 1–20.
- [32] J. R. Darwent, *J. Chem. Soc. Faraday Trans. 2* **1981**, *77*, 1703–1709.
- [33] T. Thurston, J. Wilcoxon, *J. Phys. Chem. B* **1999**, *103*, 11–17.
- [34] X. Zong, Y. Na, F. Wen, G. Ma, J. Yang, D. Wang, Y. Ma, M. Wang, L. Sun, C. Li, *Chem. Commun.* **2009**, 4536–4538.
- [35] A. N. Enyashin, L. Yadgarov, L. Houben, I. Popov, M. Weidenbach, R. Tenne, M. Bar-Sadan, G. Seifert, *J. Phys. Chem. C* **2011**, *115*, 24586–24591.
- [36] T. F. Yeh, J. M. Syu, C. Cheng, T. H. Chang, H. Teng, *Adv. Funct. Mater.* **2010**, *20*, 2255–2262.
- [37] a) L. Panchakarla, K. Subrahmanyam, S. Saha, A. Govindaraj, H. Krishna-murthy, U. Waghmare, C. Rao, *Adv. Mater.* **2009**, *21*, 4726–4730; b) X. Wang, G. Sun, P. Routh, D. H. Kim, W. Huang, P. Chen, *Chem. Soc. Rev.* **2014**, *43*, 7067–7098; c) R. Lv, M. Terrones, *Mater. Lett.* **2012**, *78*, 209–218.
- [38] Z.-R. Tang, Y. Zhang, N. Zhang, Y. J. Xu, *Nanoscale* **2015**, *7*, 7030–7034.
- [39] J. Ran, T. Y. Ma, G. Gao, X. W. Du, S. Z. Qiao, *Energy Environ. Sci.* **2015**, *8*, 3708–3717.
- [40] M. Latorre-Sánchez, A. Primo, H. García, *Angew. Chem. Int. Ed.* **2013**, *52*, 11813–11816; *Angew. Chem.* **2013**, *125*, 12029–12032.
- [41] K. Y. Lee, D. J. Mooney, *Prog. Polym. Sci.* **2012**, *37*, 106–126.
- [42] S. Wang, L. Zhang, Z. Xia, A. Roy, D. W. Chang, J. B. Baek, L. Dai, *Angew. Chem. Int. Ed.* **2012**, *51*, 4209–4212; *Angew. Chem.* **2012**, *124*, 4285–4288.
- [43] R. K. Upadhyay, N. Soin, S. S. Roy, *RSC Adv.* **2014**, *4*, 3823–3851.

Manuscript received: November 3, 2015

Accepted Article published: January 24, 2016

Final Article published: February 2, 2016